Journal of Asian Earth Sciences 251 (2023) 105653

Contents lists available at ScienceDirect

Journal of Asian Earth Sciences

journal homepage: www.elsevier.com/locate/jseaes

Evaluating the role of tectonic setting in new continental crust formation by Pb isotopic ratios

Xian Chen [a], Rui-Zhong Hu [a,b,*], Xuan-Ce Wang [c,d,*], Liang Liu [a]

[a] State Key Laboratory of Ore Deposit Geochemistry, Institute of Geochemistry, Chinese Academy of Sciences, Guiyang 550081, China
[b] College of Earth and Planetary Sciences, University of China Academy of Sciences, Beijing 100049, China
[c] School of Earth Sciences, Yunnan University, Kunming 650500, China
[d] School of Earth and Environmental Sciences, The University of Queensland, QLD 4072, Australia

ARTICLE INFO

Keywords:
New crust formation
Tectonic setting
I-type granitoids
Nd-Pb isotopes
$^{206}Pb/^{204}Pb$ ratios

ABSTRACT

How new continental crust formed remains a matter of debate. A key to solve this issue is to determine which tectonic setting(s) are involved in new crust formation. Modern mantle-derived magmas that formed in intracontinental extension settings (OIB-like U/Pb = ~0.28–0.37) and in subduction settings (IAB-like U/Pb = ~0.1–0.16) have distinct mean U/Pb ratios, furthermore, the mean U/Pb (~1.8–2.0) of depleted mantle (DM) is mainly between the OIB-like and IAB-like U/Pb ratios. Therefore, the Pb isotopic ratios (e.g., $^{206}Pb/^{204}Pb$) of subduction-related mantle-derived magmas develop below the lead isotopic evolution curve of depleted mantle (DM), whereas those ratios of mantle-derived magmas generated in intracontinental extension settings evolve above the DM evolution curve. Here we used published Nd-Pb isotope compositions from 75 I-type granitoid samples to calculate the time of new crust formation (T_{DM}) and $^{206}Pb/^{204}Pb$ ratios [$(^{206}Pb/^{204}Pb)_t$] of new crust at t (i.e., time of new crust remelting) in the Songliao Block from East Asia to determine tectonic settings in which new crust formed have changed with time. Our results show that $(^{206}Pb/^{204}Pb)_t$ ratios corresponding to T_{DM} of ~ 1.55–1.2 Ga plot below the DM evolution curve, indicating a subduction setting of new crust formation, whereas, the $(^{206}Pb/^{204}Pb)_t$ ratios corresponding to T_{DM} of ~ 1.05–0.70 Ga plot above the DM evolution curve, indicating an intracontinental extension setting of new crust formation. Hence, here two distinct tectonic settings of new crust formation are recognized in the Songliao Block. In addition, this method is also applied to well determine the tectonic settings of new crust formation in the Jibei area of North China and the Qinling area of Central China during the Paleoproterozoic (ca. 2.2–1.8 Ga). Therefore, our study demonstrates that the calculation of T_{DM} and $(^{206}Pb/^{204}Pb)_t$ ratios of new continental crust from the bulk-rock record may constitute a potential approach to better constrain how new continental crust formed and the Precambrian tectonic evolution of continents.

1. Introduction

Although the timing of crust formation has been constrained by Nd and Hf isotopes (e.g., Dhuime et al., 2012; Condie et al., 2018), the mechanism of new continental crust formation in different places at different stages of Earth's evolution remains a matter of debate (Moresi et al., 2014; Wang et al., 2020). The average andesitic composition of the bulk continental crust (BCC), coupled with the magnificent andesite volcanism which occurs at subduction zones, and similar incompatible element patterns between BCC and arc magmas (Rudnick, 1995; Davidson and Arculus, 2006; Niu et al., 2013), lead to the "island arc" model widely accepted for the origin of the continental crust. However, this model cannot explain some crucial geological characteristics: e.g., (i) the bulk arc crust (BAC) is basaltic whereas the BCC is andesitic (Niu et al., 2013); (ii) Th/U ratio, Cr, Ni (Taylor and McLennan, 1985) and Sr contents (Niu et al., 2013) are distinct between BAC and BCC; (iii) BAC contributes no net mass to the BCC growth, at least in the Phanerozoic (Niu et al., 2013); (iv) It also difficultly explains continental crust growth in early earth (Moresi et al., 2014). For example, >65% of the present volume of continental crust might be generated before 3 Ga (Dhuime et al., 2012; Hawkesworth et al., 2019), when geodynamic modes other than plate tectonics may have been operating (Cawood et al., 2018). In contrast, an alternate model of crustal growth by vertical growth in extension settings has been invoked in response to plume-

* Corresponding authors at: State Key Laboratory of Ore Deposit Geochemistry, Institute of Geochemistry, Chinese Academy of Sciences, Guiyang 550081, China (R.H.); School of Earth Sciences, Yunnan University, Kunming 650500, China (X.W.).
E-mail addresses: huruizhong@vip.gyig.ac.cn (R.-Z. Hu), x.wang4@uq.edu.au (X.-C. Wang).

https://doi.org/10.1016/j.jseaes.2023.105653
Received 4 January 2023; Received in revised form 23 March 2023; Accepted 27 March 2023
Available online 31 March 2023
1367-9120/

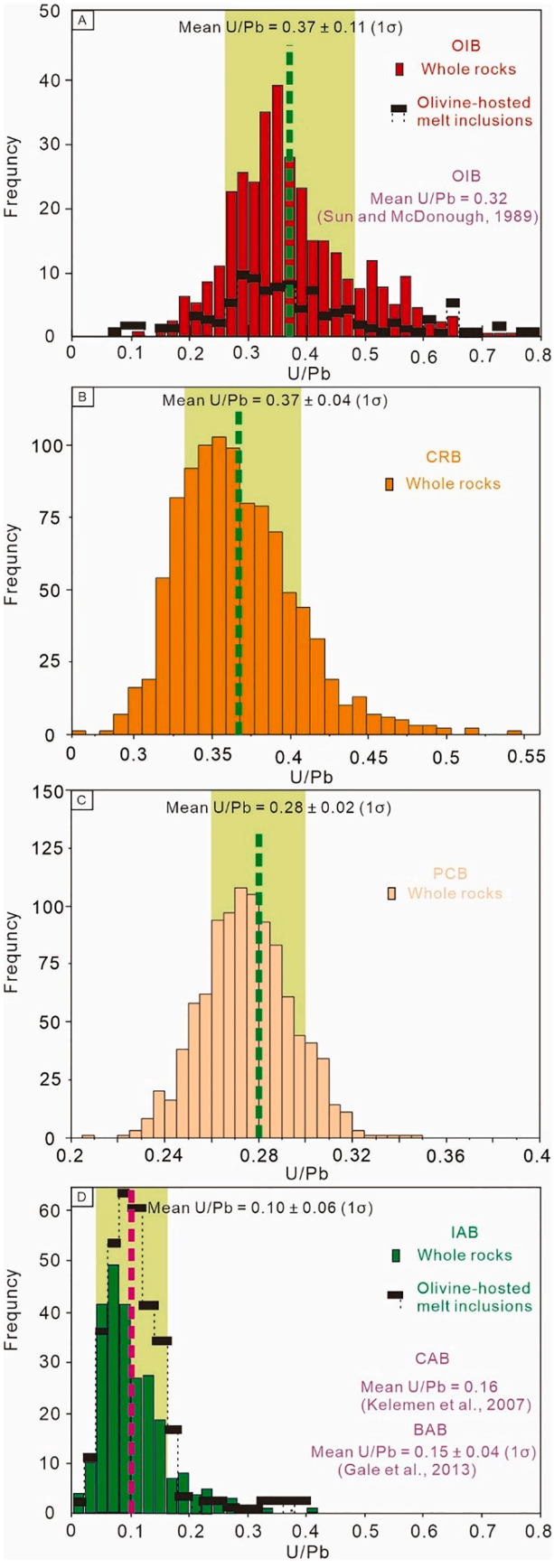

(caption on next column)

Fig. 1. (A–D) Present-day distribution of U/Pb ratios of basalts in intracontinental extension (OIB-like) and subduction (IAB-like) settings. Data for IAB and OIB are from Delavault et al. (2016). Data for BAB and CAB are from Gale et al. (2013) and Kelemen et al. (2007), respectively. Data for PCB are from Aldanmaz et al. (2000); Duggen et al. (2005); Aydınçakır and Şen (2013); Pang et al. (2013); Kheirkhah et al. (2015); Erturk et al. (2017). Data for CRB are from the GEOROC database (http://georoc.mpch-mainz.gwdg.de/georoc/, Table S1). IAB-like = IAB, CAB, BAB. IAB—Island arc basalt, CAB—Continental arc basalt, BAB—Back-arc basalt. OIB-like = OIB, CRB, PCB. OIB—Ocean island arc basalt, CRB—Continental rift basalt, PCB—Post-collisional basalt.

related and/or intracontinental extensional magmatism (Frost et al., 2001; Couzinié et al., 2016), but its role in new continental formation is not well constrained (Albarède, 1998). Hence, the key to reveal the mechanism of new continental crust formation is to determine which tectonic setting(s) are involved in the generation of new continental crust through time.

Accretionary mountain belts, such as Central Asian Orogenic Belt (CAOB), record major growth of continental crust by the addition of juvenile magmas, which can be used to determine how new crust formed (Cawood et al., 2009). The Songliao Block, located within the CAOB, formed through a long-lived accretionary phase involving episodes of subduction, collision, and extension during the Precambrian (Luan et al., 2019). Therefore, it is an ideal natural laboratory for studying mechanisms of new crust formation. This study applies previous Pb-Nd isotope compositions of I-type granitoids from across the microcontinent to investigate the role tectonic setting in the generation of new continental crust.

2. Method

Uranium is much more incompatible than Pb during mantle partial melting that produced OIB and MORB (Hofmann, 2003), whereas fluid-mobile Pb is more readily transported during mantle partial melting enriched in water at subduction zones resulting in the marked decrease of U/Pb of magmas (Kogiso et al., 1997). Hence, modern primitive mantle–derived magmas generated in intracontinental extension settings and in subduction settings have distinct mean U/Pb ratios (Fig. 1A-D). Overall primary magmas formed in intraplate settings (OIB-like) have higher mean U/Pb ratios (e.g., Ocean island basalt, ~0.37 ± 0.11 (1σ), Delavault et al., 2016, or ~ 0.32 Sun and McDonough, 1989; Continental rift basalt, ~0.37 ± 0.04 (1σ), Table S1, and Post-collision basalt, ~0.28 ± 0.02 (1σ), Aldanmaz et al., 2000; Duggen et al., 2005; Aydınçakır and Şen, 2013; Pang et al., 2013; Kheirkhah et al., 2015; Erturk et al., 2017. Fig. 1A-C), whereas primary magmas generated in subduction settings (IAB-like) have lower mean U/Pb ratios (Island arc basalt, ~0.10 ± 0.06 (1σ), Delavault et al., 2016; Continental arc basalt, ~0.16, Kelemen et al., 2007; Back-arc basalt, ~0.15 ± 0.04 (1σ), Gale et al., 2013). In addition, depleted mantle (DM) have mean U/Pb ratios of 0.18 (Workman and Hart, 2005), or 0.20 (Salters and Stracke, 2004). Delavault et al. (2016) used the Pb isotope record of feldspar inclusions in zircon and zircon-Hf model ages to calculate the U/Pb ratios of the mafic protoliths of two granite samples [i.e., juvenile mafic crust $(U/Pb)_{jc}$], to reveal the tectonic settings of new crust formation, demonstrating the potential of calculating $(U/Pb)_{jc}$ in determining the tectonic settings of new crust formation. However, there are relatively big uncertainties in the calculation of $(U/Pb)_{jc}$, because of the involvement of the parameters with big uncertainties, such as $^{238}U/^{204}Pb$ (~1.09–9.72, Sun and McDonough, 1989; Rehkamper and Hofmann,1997; Salters and Stracke, 2004; Workman and Hart, 2005; Gale et al., 2013) and $^{206}Pb/^{204}Pb$ (~18.00–18.298, Rehkamper and Hofmann, 1997; Gale et al., 2013) of depleted mantle, furthermore, it remains difficult to obtain high precision data for a large number of representative samples. Hence, here we present an improved method to avoid the calculation of $(U/Pb)_{jc}$. Because OIB-like and IAB-like magmas have distinct U/Pb ratios, Pb isotopic ratios (e.g., $^{206}Pb/^{204}Pb$) of subduction-related

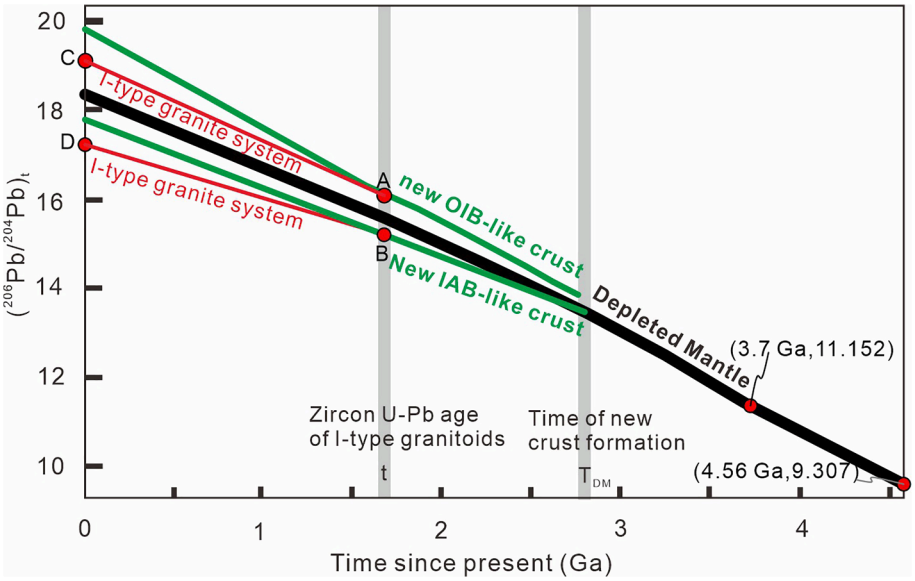

Fig. 2. Evolution of the $^{206}Pb/^{204}Pb$ ratios through time: Black, red and green lines represent the evolution paths of depleted mantle (DM), I-type granitoids and new continental crust, respectively. A and B reflect the remelting of new OIB-like crust and IAB-like crust at t, respectively. C and D represent present day $^{206}Pb/^{204}Pb$ ratios of I-type granite samples formed through the remelting of new OIB-like crust and IAB-like crust, respectively. (For interpretation of the references to colour in this figure legend, the reader is referred to the web version of this article.)

primary mantle-derived magmas (IAB-like) should mainly develop below the lead isotopic evolution curve of depleted mantle (DM), whereas those ratios of primary mantle-derived magmas (OIB-like) generated in intracontinental extension settings should evolve above the DM evolution curve (Fig. 2). Here we calculate $^{206}Pb/^{204}Pb$ ratios [$(^{206}Pb/^{204}Pb)_t$] of new continental crust remelting at t (crystallization time of felsic magma) and time of new crust formation (T_{DM}) to determine which tectonic setting(s) are involved in the generation of new continental crust through time (Fig. 2).

The $(^{206}Pb/^{204}Pb)_t$ ratio and T_{DM} can be calculated from the U-Pb age and the Pb-Nd isotopic compositions of I-type granitoids, using the following Equations:

$$(^{206}Pb/^{204}Pb)_t = (^{206}Pb/^{204}Pb)_s - (^{238}U/^{204}Pb)_s*(e^{\lambda 1t} - 1) \quad (1)$$

$$\mu = (^{238}U/^{204}Pb)_s = (U/Pb)_s*M_{Pb}*\omega_U^{238}/(M_U*\omega_{pb}^{204}) = (U/Pb)_s/0.016 \quad (2)$$

$$f_{Sm/Nd} = \left[\left(^{147}Sm/^{144}Nd\right)_s/\left(\left(^{147}Sm/^{144}Nd\right)_{CHUR}\right)\right] - 1 \quad (3)$$

$$T_{DM1} = 1/\lambda_2 \times \ln\{[(^{143}Nd/^{144}Nd)_s - (^{143}Nd/^{144}Nd)_{DM}]/[(^{147}Sm/^{144}Nd)_s - (^{147}Sm/^{144}Nd)_{DM}] + 1\} \quad (4)$$

$$T_{DM2} = T_{DM1} - (T_{DM1} - t)[(fc - fs)/(fc - f_{DM})] \quad (5)$$

where t is the U-Pb crystallization age of zircon; $(^{206}Pb/^{204}Pb)_t$ is the Pb isotope compositions of new crust at t; $(^{206}Pb/^{204}Pb)_s$ and $(^{238}U/^{204}Pb)_s$ are the measured $^{206}Pb/^{204}Pb$ and $^{238}U/^{204}Pb$ ratios of I-type granite samples, respectively; $(^{238}U/^{204}Pb)_s$ can be calculated by whole-rock U/Pb of I-type granite samples; λ_1 is the decay constant of ^{238}U ($1.55125 \times 10^{-10}.yr^{-1}$). M_{Pb} and M_U represent standard atomic weights of Pb and U, respectively. ω_{Pb}^{204} and ω_U^{238} represent the relative abundances of ^{204}Pb as percent of total Pb and ^{238}U as percent of total U, respectively. The Pb isotope evolution of the mantle was calculated from the composition of the Canyon Diablo troilite at $t_0 = 4560$ Ma and a two-stage model similar to that of Stacey and Kramers (1975), in which $(^{206}Pb/^{204}Pb)_{4560Ma} = 9.307$, $(^{206}Pb/^{204}Pb)_{(4560\sim3700Ma)} = 11.152$, to

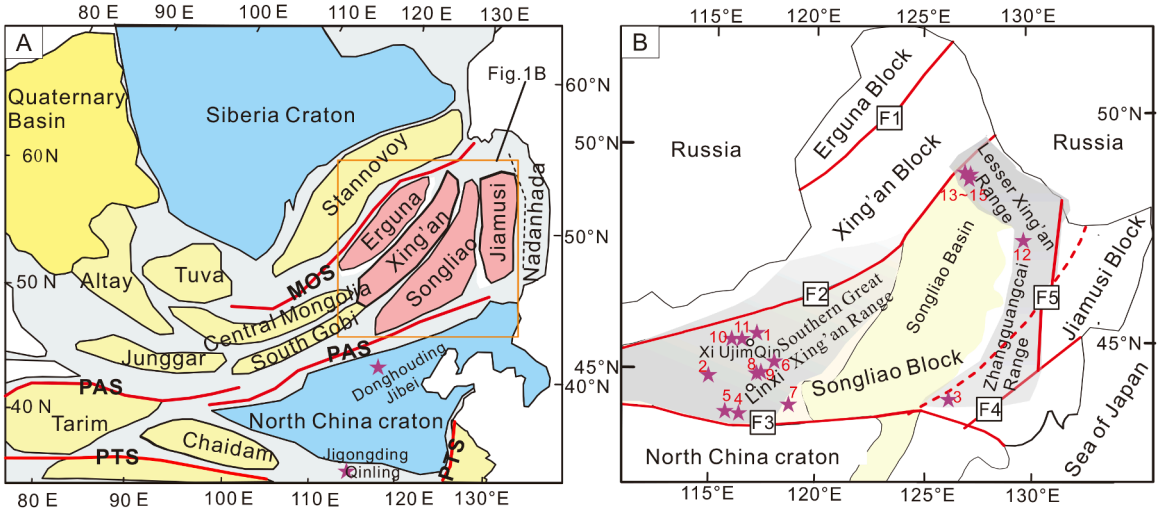

Fig. 3. (A) Sketch tectonic map of Asia (modified after Zhou et al., 2009). (B) Simplified tectonic map of NE China (modified from Zhou et al., 2009). MOS: Mongol-Okhotsk suture; PAS: Paleo-Asian suture; PTS: Paleo-Tethys suture; F1: Tayuan-Xiguitu Fault; F2: Hegenshan-Heihe Fault; F3: Solonker-Xar Moron-Changchun-Yanji Fault; F4: Dunhua-Mishan Fault; F5: Jiayin-Mudanjiang Fault. Red dashed line in Fig. 2B represents secondary faults. Pentangle in Fig. 2B represents sample location. (For interpretation of the references to colour in this figure legend, the reader is referred to the web version of this article.)

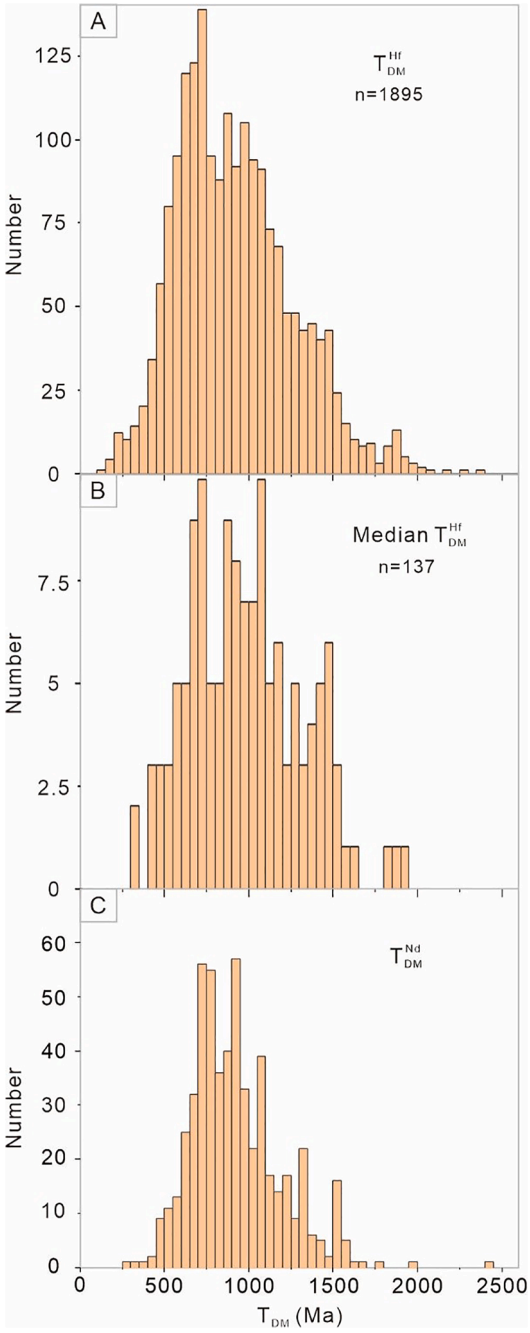

Fig. 4. Relative probability plots of zircon-Hf (A-B) and whole-rock Nd (C) model ages of granitoids from the Songliao Block. A. Hf model ages of all zircons data from the granitoids in the Songliao Block; B. median values of Hf model ages of the analytical zircons from the granitoids in the Songliao Block. Data are from Tables S2 and S3.

match present-day mean $(^{206}Pb/^{204}Pb)_{DM} = 18.298$ (Gale et al., 2013). In addition, $(^{143}Nd/^{144}Nd)_s$ and $(^{147}Sm/^{144}Nd)_s$ are the measured values of I-type granite samples; λ_2 is the decay constant of ^{147}Sm (6.54×10^{-6} $m.y^{-1}$); $(^{143}Nd/^{144}Nd)_{DM} = 0.513151$; $(^{147}Sm/^{144}Nd)_{DM} = 0.2137$; $(^{143}Nd/^{144}Nd)_{CHUR} = 0.512638$; $(^{147}Sm/^{144}Nd)_{CHUR} = 0.1967$; $(^{147}Sm/^{144}Nd)_{cc} = 0.118$. When $f_{Sm/Nd} = -0.5 \sim -0.3$ and $f_{Sm/Nd} < -0.5$ or > -0.3, T_{DM} use the value of T_{DM1} and T_{DM2} respectively. So that, the Nd model age (T_{DM}) is close to the real model age of one sample as far as possible (Yang et al., 2017).

3. Geological background

The Songliao Block, NE China, lies in the eastern CAOB and contains the Lesser Xing'an-Zhangguangcai Range in the east, the southern Great Xing'an Range in the west, and the central Songliao Basin (Fig. 3A-B) (Zhou et al., 2009). The tectonic evolution of this microcontinent is controlled by the Paleo-Asian Ocean system in the Paleozoic, followed by subduction of the Paleo-Pacific Plate since the early Jurassic (Zhou et al., 2009). It may have experienced three or four phases of collisional orogenesis with the adjacent plates during the Phanerozoic (Xu et al., 2013), which resulted in the destruction/recycling of large amounts of old crustal material. The exposed Precambrian basement is sparsely distributed in the east, northwest and south of the microcontinent, and it is mainly composed of Neoproterozoic metamorphic units (~0.6–0.9 Ga) with minor Paleoproterozoic (~1.8 Ga) and the Neoarchean (~2.7 Ga) metamorphic granitoids (Wu et al., 2018; Zhang et al., 2018; Luan et al., 2019). In addition, Paleoproterozoic (~2.1–1.9 Ga) continental lithospheric mantle occurs in the northeast of the block (Zhang et al., 2011). Thus, ancient Precambrian crystalline basement existed in the microcontinent, but most of them might be strongly destructed in the multiple phases of orogenesis during the Phanerozoic. The microcontinent contains abundant Paleozoic-Mesozoic granitoids and Phanerozoic sedimentary formations (Wu et al., 2011). The granitoids are dominated by I- and A-types, with no documented S-type (Wu et al., 2011). The growth timing of this microcontinent was constrained by Nd-Hf isotopes and the Mesoproterozoic and the Neoproterozoic are the two main periods of new continental crust formation in the microcontinent (Tables S2 and S3, Fig. 4A–C). However, the mechanism of new crust formation, as well as its Precambrian tectonic evolution remain unclear, because of the absence of ancient igneous rocks related to crustal accretion.

4. Sample selection and calculated result

4.1. Sample selection

On the basis of the above five calculation formulas (Eqs. (1)–(5)), the fractionation of I-type granitoids does not impact the calculation of T_{DM} and $(^{206}Pb/^{204}Pb)_t$ ratios of new crust. However, generally, the calculation of T_{DM} and $(^{206}Pb/^{204}Pb)_t$ ratios of new crust can be impacted by the significant processes (e.g., contamination, magma mixing and alteration). Hence, the I-type granitoid samples with high loss on ignition, marked contamination and magma mixing are not suitable for our method. We collect whole-rock major/trace elements and Nd-Pb isotope data of I-type granitoids, when there are $n \geq 3$ analyses for each I-type felsic pluton or volcanic rock. So that we can determine whether the granitoid samples have been modified by the potential geologecal processes such as contamination, alteration, magma mixing. Hence, the I-type granitoid samples with $n \leq 2$ analyses for each I-type felsic pluton or volcanic rock, marked contamination [e.g., wide ranges of $\varepsilon_{Nd}(t)$], alteration (e.g., LOI > 3 wt%), magma mixing (e.g., samples with enclaves) are excluded in our study. Here 15 different I-type granitoids from the Songliao Block are included in our study (Table S4, Fig. 3).

4.2. Calculated result

Here we calculated the time of new crust formation (T_{DM}) and $(^{206}Pb/^{204}Pb)_t$ ratios using the Nd-Pb isotopic compositions of 75 published well-dated samples from 15 different granitoids, namely, 281 Ma rhyolite, 279 Ma rhyolite, 253 Ma andesite, 251 Ma andesite, 186 Ma monzogranite, 181 Ma rhyolite, 168 Ma granodiorite porphyry, 157 Ma rhyolite, 156 Ma rhyolite, 147 Ma monzogranite, 143 Ma syenogranite porphyry, 138 Ma monzogranite, and 139 Ma granite, 120 Ma andesite, 119 Ma granite porphyry and 112 Ma dacite respectively, in the Songliao Block (Table S4). These rock samples are relatively fresh with SiO_2 of 55.25–78.12 wt%, low loss on ignition (LOI) (0.26–2.98 wt%),

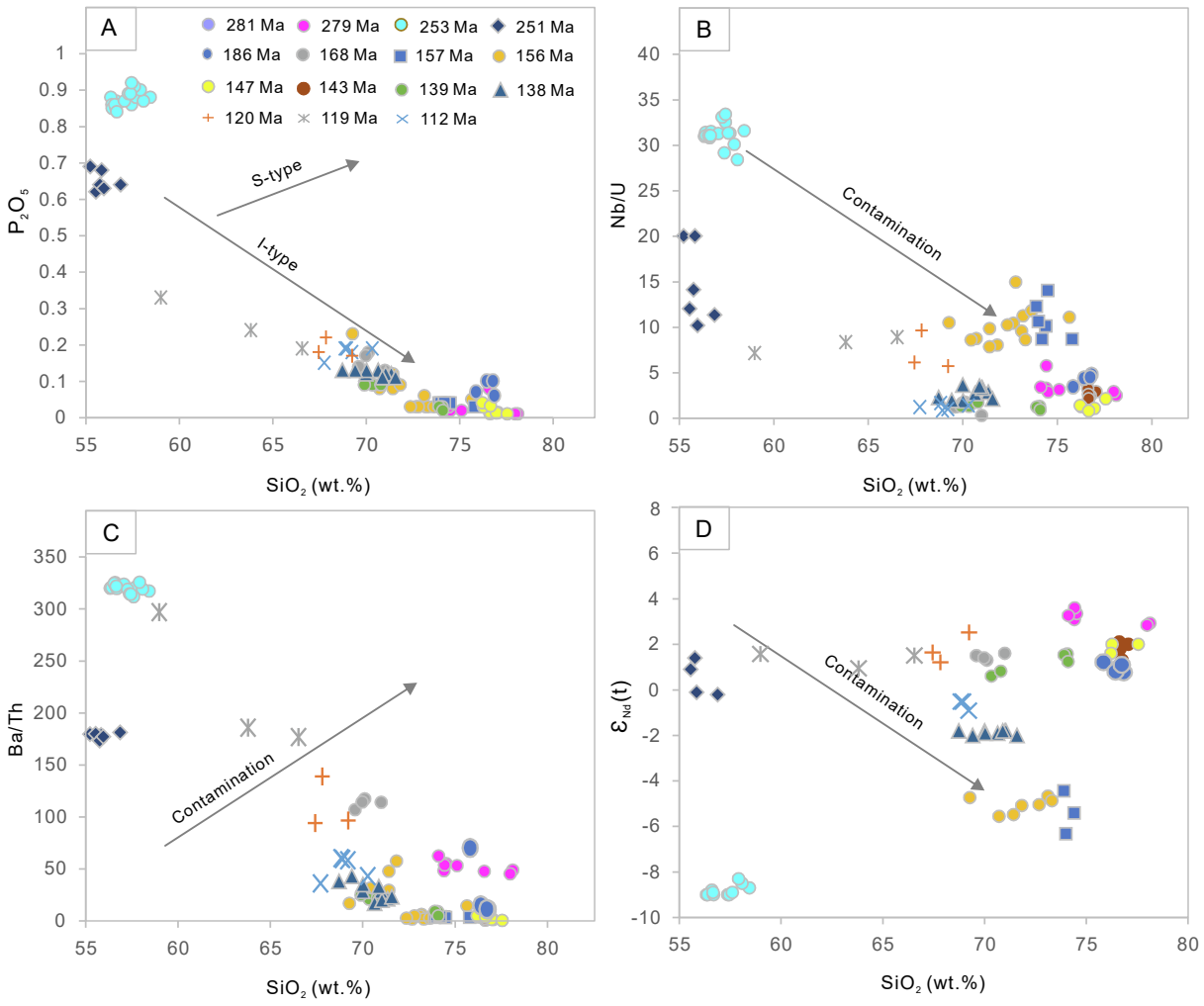

Fig. 5. Plots of (A) P_2O_5 vs. SiO_2, (B) Nb/U vs. SiO_2, (C) Ba/Th vs. SiO_2, and (D) $\varepsilon_{Nd}(t)$ vs. SiO_2 for the I-type granitoid samples in the Songliao Block. Data are shown in Table S5.

characterized by I-type granitoids (Table S5, Fig. 5A). In addition, individual granitoid samples display narrow variation of Nb/U, Ba/Th and $\varepsilon_{Nd}(t)$ with the increasing of SiO_2 (Table S5, Fig. 5B-D).

The calculated results show T_{DM} of ~ 0.88–0.90 Ga and $(^{206}Pb/^{204}Pb)_t$ of 18.235 ~ 18.748 for the 281 Ma rock samples; T_{DM} of ~ 0.75–0.8 Ga and $(^{206}Pb/^{204}Pb)_t$ of 17.807 ~ 18.217 for the 279 Ma

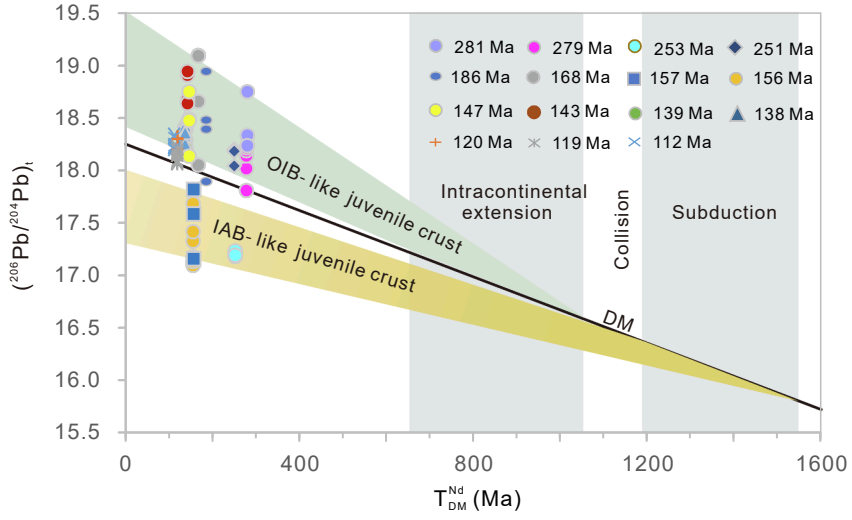

Fig. 6. Plot of $(^{206}Pb/^{204}Pb)_t$ vs. T_{DM}. T_{DM} represents the time of new crust formation. $(^{206}Pb/^{204}Pb)_t$ represents the $^{206}Pb/^{204}Pb$ ratio of new crust at t. Data are shown in Table S4.

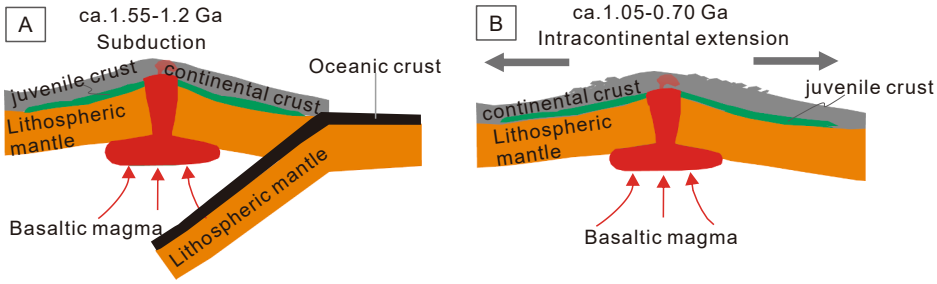

Fig. 7. Tectonic settings of new crust formation in the Songliao Block during the Meso-Neoproterozoic.

rock samples; T_{DM} of ~ 1.45–1.55 Ga and $(^{206}Pb/^{204}Pb)_t$ of 17.18 ~ 17.23 for the 253 Ma rock samples; T_{DM} of ~ 0.75–0.85 Ga and $(^{206}Pb/^{204}Pb)_t$ of 18.04 ~ 18.20 for the 251 Ma rock samples; T_{DM} of ~ 1.04–1.07 Ga and $(^{206}Pb/^{204}Pb)_t$ of 17.896 ~ 18.946 for the 186 Ma monzogranite samples; T_{DM} of ~ 0.77–0.78 Ga and $(^{206}Pb/^{204}Pb)_t$ of 18.049 ~ 19.096 for the 168 Ma rock samples; T_{DM} of ~ 1.3–1.45 Ga and $(^{206}Pb/^{204}Pb)_t$ of 17.156 ~ 17.817 for the 157 Ma rock samples; T_{DM} of ~ 1.2–1.35 Ga and $(^{206}Pb/^{204}Pb)_t$ of 17.092 ~ 17.683 for the 156 Ma rock samples, T_{DM} of ~ 0.8–1.0 Ga and $(^{206}Pb/^{204}Pb)_t$ of 18.134 ~ 18.748 for the 147 Ma monzogranite samples, T_{DM} of ~ 0.8 ~ 0.9 Ga and $(^{206}Pb/^{204}Pb)_t$ of 18.636 ~ 18.942 for the 143 Ma syenogranite porphyry samples, T_{DM} of ~ 0.8–1.05 Ga and $(^{206}Pb/^{204}Pb)_t$ of 18.174 ~ 18.398 for the 139 Ma granite samples, T_{DM} of ~ 0.9–1.05 Ga and $(^{206}Pb/^{204}Pb)_t$ of 18.253 ~ 18.485 for the 138 Ma monzogranite samples, T_{DM} of ~ 0.72–0.79 Ga and $(^{206}Pb/^{204}Pb)_t$ of 18.202 ~ 18.302 for the 120 Ma andesite samples, T_{DM} of ~ 0.70–0.74 Ga and $(^{206}Pb/^{204}Pb)_t$ of 18.158 ~ 18.194 for the 119 Ma granite porphyry samples, and T_{DM} of ~ 0.70–0.90 Ga and $(^{206}Pb/^{204}Pb)_t$ of 18.209 ~ 18.325 for the 112 Ma dacite samples, respectively (Table S4).

5. Discussion

Here our compiled I-type granitoid samples display relatively low LOI (<3 wt%), narrow variation of Nb/U, Ba/Th and $\varepsilon_{Nd}(t)$ with the increasing of SiO_2 (Table S5, Fig. 5B-D). Furthermore, we do not find other potential evidence of magma mixing [e.g., mafic enclaves, large variation of $\varepsilon_{Nd}(t)$] in these I-type granitoid samples. Hence, the potential processes, such as contamination, magma mixing and alteration, might not have a significant impact on the calculation of T_{DM} and $(^{206}Pb/^{204}Pb)_t$ ratios of new crust in this study. As a result, they can be used to evaluate the tectonic settings of new crust formation through Nd-Pb isotopic compositions.

As stated above, the results show $(^{206}Pb/^{204}Pb)_t$ ratios corresponding to T_{DM} of ~ 1.55–1.2 Ga plot below the DM evolution curve [$(^{206}Pb/^{204}Pb)_t$ = 17.09 ~ 17.82], whereas, the $(^{206}Pb/^{204}Pb)_t$ ratios corresponding to T_{DM} of ~ 1.05–0.70 Ga plot above the DM evolution curve [$(^{206}Pb/^{204}Pb)_t$ = 17.81 ~ 19.10] (Fig. 6). This implies that new crust was generated in a subduction setting during ~ 1.55–1.20 Ga, however, in an intracontinental extension setting during ~ 1.05–0.70 Ga (Fig. 7). Hence, here two distinct tectonic settings of new crust formation are recognized in the Songliao Block. This conclusion is consistent with reconstruction models of Rodinia assembly and the subsequent

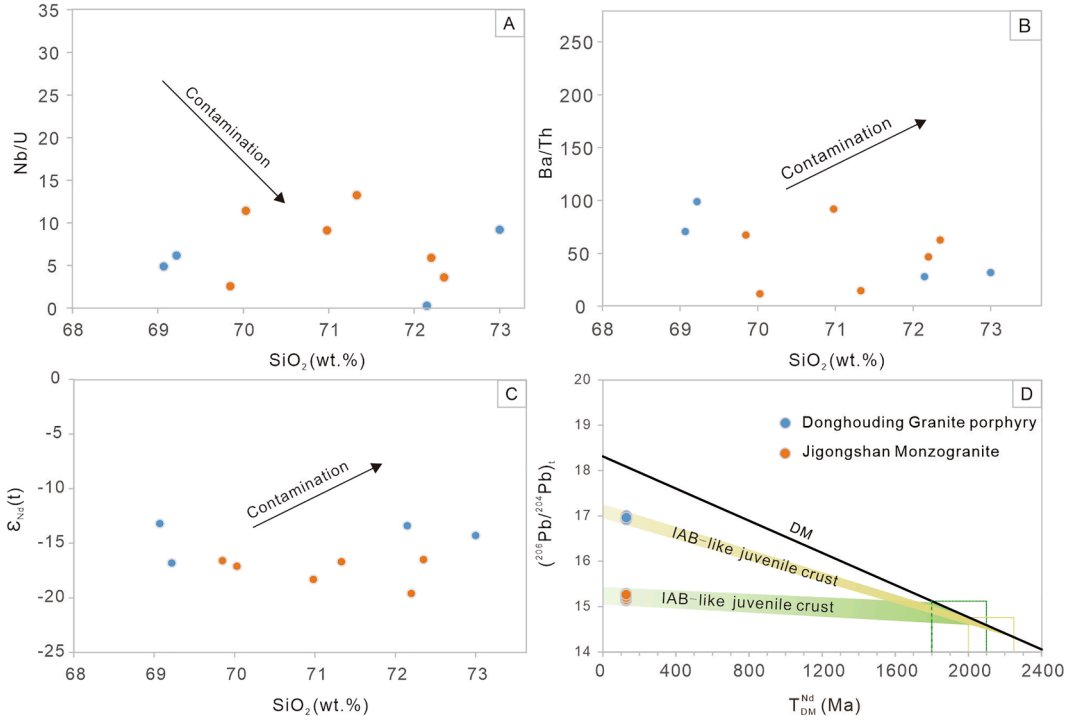

Fig. 8. Plots of (A) Nb/U vs. SiO_2, (B) Ba/Th vs. SiO_2 and (C) $\varepsilon_{Nd}(t)$ vs. SiO_2, and (D) $(^{206}Pb/^{204}Pb)_t$ vs. T_{DM} of new crust for the Donghouding and Jigongshan granitic plutons from the Jibei area of North China and Qinling area of Central China, respectively. T_{DM} represents the time of new crust formation. $(^{206}Pb/^{204}Pb)_t$ represents the $^{206}Pb/^{204}Pb$ ratio of new crust at t. Data are shown in Tables S4 and S5.

extension of some continents during the late Mesoproterozoic-Neoproterozoic (Li et al., 2008). For example, the Cathaysia and South Tarim, potentially near or connected to each other, likely joined Rodinia northern Australia during 1.3–1.0 Ga (Zhao et al., 2021). Coincidentally, detrital zircons from the Songliao and Tarim Blocks have similar age spectra in the Precambrian (Chen, 2018), indicating similar evolution for them at that time. Hence, the Songliao Block might also be a part of the Rodinia.

In addition, in order to verify the feasibility of this method, we calculate T_{DM} values and $(^{206}Pb/^{204}Pb)_t$ ratios of new crust from the Jibei area of North China during ca. 2.2–2.0 Ga and from the Qinling area of Central China during ca. 2.1–1.8 Ga (Table S4). The Donghouding granite porphyry (129 Ma) from Jibei area (Liang et al., 2013) and the Jigongshan monzogranite (128 Ma) from Qinling area (Zhang et al., 2004) are used to carry out further study. Both of them are predominantly derived from the remelting of prior mafic crust rather than sedimentary rocks (Zhang et al., 2004; Liang et al., 2013). They have low LOI (<2 wt%), weak variation of Nb/U, Ba/Th and $\varepsilon_{Nd}(t)$ with the rise of SiO_2 (Fig. 8A-C, Table S5), hence, these granites are probably not significantly modified by the processes such as contamination, magma mixing and alteration. They can be used to calculate T_{DM} values and $(^{206}Pb/^{204}Pb)_t$ ratios of new crust. Calculated results show T_{DM} of 2258 ~ 2007 Ma and $(^{206}Pb/^{204}Pb)_t$ of 16.91 ~ 17.00 for four Donghouding granite samples, and T_{DM} of 2100 ~ 1800 Ma and $(^{206}Pb/^{204}Pb)_t$ of 15.13 ~ 15.29 for six Jigongshan granite samples. Significantly, all $(^{206}Pb/^{204}Pb)_t$ ratios plot below the DM evolution curve (Fig. 8D), which indicates that new crust is generated in subduction settings in the two areas during the Paleoproterozoic (~2.2–1.8 Ga), corresponding to the convergence of the Columbia/Nuna supercontinent in North China and western South China (Yangtze plate) (Zhang et al., 2004; Zhao and Cawood, 2012; Wang et al., 2016). Therefore, this method is also applied to well determine the tectonic settings of new crust formation in the two regions during the Paleoproterozoic (ca. 2.2–1.8 Ga).

In addition, note that generally, the samples with $(^{206}Pb/^{204}Pb)_t$ ratios plotted away from Pb isotopic evolution line of the DM can suit well for this method. If significant processes such as contamination, alteration and magma mixing can be excluded in the samples with relatively obvious variation of $(^{206}Pb/^{204}Pb)_t$ ratios, the tectonic setting of new crust formation should be identified based on the overall distribution of $(^{206}Pb/^{204}Pb)_t$ data below or above the DM evolution line rather than individual data. So that we can preclude the interference of the $(^{206}Pb/^{204}Pb)_t$ data plotted near the DM evolution line. If all $(^{206}Pb/^{204}Pb)_t$ data of individual granitoid samples plot near the DM evolution line, the primary magmas of the granitoid samples might be Depleted mantle-derived and formed through the fractionation of basaltic magmas. Hence, our method might bring a good perspective to the studies of I-type granitoids associated with the regimes of crust growth and the Precambrian tectonic evolution of continents.

6. Conclusion

This study employs the calculation of time of new crust formation (T_{DM}) and $(^{206}Pb/^{204}Pb)_t$ ratios of new crust to constrain the regimes of new continental crust formation.

(1) Two distinct regimes of new crust formation (i.e., through subduction during ~ 1.55–1.2 Ga and intracontinental extension during ~ 1.05–0.70 Ga) are recognized in the Songliao Block of East Asia.
(2) This method is also applied to well determine the tectonic settings of new crust formation in the Jibei area of North China and the Qinling area of Central China during the Paleoproterozoic (~2.2–1.8 Ga).
(3) This method may provide a potential avenue to explore the regimes of new continental crust formation and the Precambrian tectonic evolution of continents.

Author contributions

Xian Chen and **Ruizhong Hu** discussed, designed the research, interpreted data; **Xian Chen** drafted the paper; **Xuance Wang** contributed to further discussion and data interpretation and revision; **Ruizhong Hu** and **Xian Chen** provided finding sources; **Liang Liu** contributed to further discussion and revision.

Declaration of Competing Interest

The authors declare that they have no known competing financial interests or personal relationships that could have appeared to influence the work reported in this paper.

Data availability

Data will be made available on request.

Acknowledgments

This work is supported jointly by the Strategic Priority Research Program (B) of the Chinese Academy of Sciences (grant number XDB18000000), the National Natural Science Foundation of China, China (grant number 41903048). We are grateful to Chris Hawkesworth, Bruno Dhuime, Peter Cawood, Peng Peng, Run-Sheng Yin, Chang-Zhou Deng, Jing-Jing Zhu and Guijuan Guo for significant discussion and help.

Appendix A. Supplementary material

Supplementary data to this article can be found online at https://doi.org/10.1016/j.jseaes.2023.105653.

References

Albarède, F., 1998. The growth of continental crust. Tectonophysics 296, 1–14.
Aldanmaz, E., Pearce, J.A., Thirlwall, M.F., Mitchell, J.G., 2000. Petrogenetic evolution of late cenozoic, post-collision volcanism in western Anatolia, Turkey. J. Volcanol. Geoth. Res. 102, 67–95.
Aydınçakır, E., Şen, C., 2013. Petrogenesis of the post-collisional volcanic rocks from the Borçka (Artvin) area: Implications for the evolution of the Eocene magmatism in the Eastern Pontides (NE Turkey). Lithos 172, 98–117.
Cawood, P.A., Kroner, A., Collins, W.J., Kusky, T.M., Mooney, W.D., Windley, B.F., 2009. Accretionary orogens through earth history. Spec. Publ. - Geol. Soc. London. 318, 1–36.
Chen, X., 2018. Crustal growth and mineralization of the granitoids in the eastern Songliao Massif, NE China. Ph. D. Dissertation. Beijing: China University of Geosciences 1-183 (in Chinese with English abstract).
Cawood, P.A., Hawkesworth, C.J., Pisarevsky, S.A., Dhuime, B., Capitanio, F.A., Nebel, O., 2018. Geological archive of the onset of plate tectonics. Philos. T. R. Soc. A. 376, 20170405.
Condie, K.C., Puetz, S.J., Davaille, A., 2018. Episodic crustal production before 2.7 Ga. Precambr. Res. 312, 16–22.
Couzinié, S., Laurent, O., Moyen, J.F., Zeh, A., Bouilhol, P., Villaros, A., 2016. Post-collisional magmatism: crustal growth not identified by zircon Hf–O isotopes. Earth Planet Sc. Lett. 456, 182–195.
Davidson, J.P., Arculus, R.J., 2006. The significance of Phanerozoic arc magmatism in generating continental crust. In: Brown, M., Rushmer, T. (Eds.), Evolution and Differentiation of the Continental Crust. Cambridge University Press, Cambridge, pp. 135–172.
Delavault, H., Dhuime, B., Hawkesworth, C.J., Cawood, P.A., Marschall, H., Facility, E.I. M., 2016. Tectonic settings of continental crust formation: insights from Pb isotopes in feldspar inclusions in zircon. Geology 44, 819–822.
Dhuime, B., Hawkesworth, C.J., Cawood, P.A., Storey, C.D., 2012. A change in the geodynamics of continental growth 3 billion years ago. Science 335, 1334–1336.
Duggen, S., Hoernle, K., Bogaard, P.V.D., Garbe-Schönberg, D., 2005. Post-collisional transition from subduction- to intraplate-type magmatism in the westernmost Mediterranean: evidence for continental-edge delamination of subcontinental lithosphere. J. Petrol. 46, 1155–1201.
Erturk, M.A., Beyarslan, M., Chung, S.L., Lin, T.H., 2017. Eocene magmatism (Maden Complex) in the Southeast Anatolian Orogenic Belt: Magma genesis and tectonic implications. Geosci. Front. 9, 1829–1847.
Frost, C.D., Bell, J.M., Frost, B.R., Chamberlain, K.R., 2001. Crustal growth by magmatic underplating: isotopic evidence from the northern Sherman batholith. Geology 29, 515–518.

Gale, A., Dalton, C.A., Langmuir, C., Su, Y., Shilling, J.G., 2013. The mean composition of ocean ridge basalts. Geochem. Geophy. Geosy. 14, 489–518.
Hawkesworth, C., Cawood, P.A., Dhuime, B., 2019. Rates of generation and growth of the continental crust. Geosci. Front. 10, 165–173.
Hofmann, A.W., 2003. Sampling mantle heterogeneity through oceanic basalts: isotopes and trace elements. Treatise Geochem. 2, 61–101.
Kelemen, P.B., Hanghøj, K., Greene, A.R., 2007. One view of the geochemistry of subduction-related magmatic arcs, with an emphasis on primitive andesite and lower crust. Treatise Geochem. 3, 749–806.
Kheirkhah, M., Neill, I., Allen, M.B., 2015. Petrogenesis of OIB-like basaltic volcanic rocks in a continental collision zone: Late Cenozoic magmatism of Eastern Iran. J. Asian Earth Sci. 106, 19–33.
Kogiso, T., Tatsumi, Y., Nakano, S., 1997. Trace element transport during dehydration processes in the subducted oceanic crust: 1. Experiments and implications for the origin of ocean island basalts. Earth Planet. Sci. Lett. 148, 193–205.
Li, Z.X., Bogdanova, S., Collins, A.S., Davidson, A., De Waele, B., Ernst, R.E., Fitzsimons, C.W., Fuck, R.A., Gladkochub, D.P., Jacobs, J., Karlstromk, K.E., Lu, S., Natapov, L.M., Pease, V., Pisarevsky, S.A., Thrane, K., Vernikovsky, V., Vernikovsky, V., 2008. Assembly, configuration, and break-up history of Rodinia: a synthesis. Precambr. Res. 160, 179–210.
Liang, Q.L., Jiang, S.H., Liu, Y.F., 2013. Petrogenesis of the Donghouding A-type Granite in Northern Hebei: constraints from Geochemistry, Zircon U-Pb Dating and Sr-Nd-Pb-Hf isotopic Composition. Geol. Rev. 59, 1120–1130 (in Chinese with English abstract).
Luan, J.P., Yu, J.J., Yu, J.L., Cui, Y.C., Xu, W.L., 2019. Early Neoproterozoic magmatism and the associated metamorphism in the Songnen Block, NE China: Petrogenesis and tectonic implications. Precamb. Res. 328, 250–268.
Moresi, L.N., Betts, P.G., Miller, M.S., Cayley, R.A., 2014. Dynamics of continental accretion. Nature 508, 245–248.
Niu, Y.L., Zhao, Z.D., Zhu, D.C., Mo, X.X., 2013. Continental collision zones are primary sites for net continental crust growth — a testable hypothesis. Earth-Sci. Rev. 127, 96–110.
Pang, K.N., Chung, S.L., Zarrinkoub, M.H., Lin, Y.C., Lee, H.Y., Lo, C.H., Khatib, M.M., 2013. Iranian ultrapotassic volcanism at ~11 Ma signifies the initiation of post-collisional magmatism in the Arabia-Eurasia collision zone. Terra Nova 25, 405–413.
Rehkamper, M., Hofmann, A.W., 1997. Recycled ocean crust and sediment in Indian Ocean MORB. Earth Planet Sci. Lett. 147, 93–106.
Rudnick, R.L., 1995. Making continental crust. Nature 378, 571–578.
Salters, V., Stracke, A., 2004. Composition of the depleted mantle. Geochem. Geophys. Geosyst. 5, Q05004.
Stacey, J.S., Kramer, J.D., 1975. Approximation of terrestrial lead isotope evolution by a two-stage model. Earth Planet. Sci. Lett. 26, 207–221.
Sun, S.S., McDonough, W.F., 1989. Chemical and isotopic systematics of oceanic basalts: implications for mantle composition and processes. Geol. Soc. Spec. Publ. 42, 313–345.
Taylor, S.R., Mclennan, S.M., 1985. The Continental Crust: Its Composition and Evolution: An Examination of the Geochemical Record Preserved in Sedimentary Rocks. Blackwell, Oxford.
Wang, W., Cawood, P.A., Zhou, M.F., Zhao, J.H., 2016. Paleoproterozoic magmatic and metamorphic events link Yangtze to northwest Laurentia in the Nuna supercontinent. Earth Planet. Sci. Lett. 433, 269–279.
Wang, X.C., Wilde, S.A., Li, Z.X., Li, S., Li, L., 2020. Do Supercontinent-Superplume Cycles control the growth and evolution of continental crust. J. Earth Sci.-China 31, 1142–1169.
Workman, R.K., Hart, S.R., 2005. Major and trace element composition of the depleted MORB mantle (DMM). Earth Planet. Sci. Lett. 231, 53–72.
Wu, F.Y., Sun, D.Y., Ge, W.C., Zhang, Y.B., Grant, M.L., Wilde, S.A., Jahn, B.M., 2011. Geochronology of the Phanerozoic granitoids in northeastern China. J. Asian Earth Sci. 41, 1–30.
Wu, X.W., Zhang, C., Zhang, Y.Q., Guo, W., Zhang, C., Cui, T.R., Yang, Y.J., Hu, J.F., Song, W.B., 2018. 2.7 Ga Monzogranite on the Songnen Block and its geological implications. Acta Geol. Sin.-Engl. 92, 1265–1266.
Xu, W.L., Pei, F.P., Wang, F., Meng, E., Ji, W.Q., Yang, D.B., Wang, W., 2013. Spatial–temporal relationships of Mesozoic volcanic rocks in NE China: constraints on tectonic overprinting and transformations between multiple tectonic regimes. J. Asian Earth Sci. 74, 167–193.
Yang, Q., Wang, T., Guo, L., Tong, Y., Zhang, L., Zhang, J., Hou, Z., 2017. Nd isotopic variation of Paleozoic-Mesozoic granitoids from the Da Hinggan Mountains and adjacent areas, NE Asia: implications for the architecture and growth of continental crust. Lithos 272, 164–184.
Zhang, Y.L., Liu, C.Z., Ge, W.C., Wu, F.Y., Chu, Z.Y., 2011. Ancient sub-continental lithospheric mantle (SCLM) beneath the eastern part of the Central Asian Orogenic Belt (CAOB): implications for crust–mantle decoupling. Lithos 126, 233–247.
Zhang, C., Wu, X.W., Liu, Z.H., Zhang, Y.J., Guo, W., Quan, J.Y., 2018. Precambrian geological events on the western margin of Songnen Block: Evidence from LA-ICP-MS U-Pb geochronology of zircons from Paleoproterozoic granite in the Longjiang area. Acta Petrol. Sin. 34, 3137–3152 (in Chinese with English abstract).
Zhang, H.F., Zhong, Z.Q., Gao, S., Zhang, B.R., Zhang, L., Hu, S.H., Hou, Q.Y., 2004. Pb and Nd isotopic composition of the Jigongshan granite: constraints on crustal structure of Tongbaishan in the middle part of the Qinling–Tongbai–Dabie orogenic belt, central China. Lithos 73, 215–227.
Zhao, G.C., Cawood, P.A., 2012. Precambrian geology of China. Precambr. Res. 222–223, 13–54.
Zhao, P., He, J., Deng, C., Chen, Y., Mitchell, R.N., 2021. Early Neoproterozoic (870–820 Ma) amalgamation of the Tarim craton (northwestern China) and the final assembly of Rodinia. Geology 49, 1277–1282.
Zhou, J.B., Wilde, S.A., Zhang, X.Z., Zhao, G.C., Zheng, C.Q., Wang, Y.J., Zhang, X.H., 2009. The onset of pacific margin accretion in NE China: evidence from the Heilongjiang high-pressure metamorphic belt. Tectonophysics 478, 230–246.